Acta Oceanol. Sin., 2023, Vol. 42, No. 7, P. 138–148
https://doi.org/10.1007/s13131-023-2193-7
http://www.aosocean.com
E-mail: ocean2@hyxb.org.cn

Nourishment and disaster mitigation efficiency of feeding sand on the dry section of a dissipative beach

Yazhuang Zhao[1, 2, 3], Hongshuai Qi[1*], Shaohua Zhao[1], Feng Cai[1], Jianhui Liu[1], Pu Xu[2], Zheyu Xiao[1], Yanyu He[1, 4], Zhiyong Zhang[1, 2]

[1] Third Institute of Oceanography, Ministry of Natural Resources, Xiamen 361005, China

[2] College of Civil Engineering, Fuzhou University, Fuzhou 350108, China

[3] Power China Huadong Engineering Corporation Limited, Hangzhou 310014, China

[4] College of Marine Geosciences, Ocean University of China, Qingdao 266100, China

Received 12 November 2022; accepted 10 March 2023

Abstract

To explore the nourishment effect and disaster reduction efficiency of a fully dissipative dry beach under the impact of storms, this paper uses the measured topography and hydrodynamic data to establish a one-dimensional numerical model of the XBeach beach profile. By numerically modeling the change in the nourished profile for different dry beach widths under normal waves and storm conditions and the recovery process of the profile after the storm, the degree of response in dry beach nourishment for the fully dissipative beach is analyzed. The results show that under normal wave conditions, the response of the nourished dry beach is obvious. Sediment on the dry beach erodes heavily, and the shoreline moves landward over a long distance. With the increase in the width and size of the dry beach, the wave height at the bottom of the backshore profile decreases, the wave height attenuation rate increases continuously, and the wave elimination effect is remarkable. When the storm incident wave intensifies, the wave height attenuation rate of the nourished dry beach decreases, indicating that the smaller the storm intensity is, the more significant the wave reduction effect of the nourished dry beach is. At the same time, different profile arrangements of nourished dry beaches suffer from different degrees of erosion under storm conditions, with significant changes in profile morphology. With intensified storm action, the intensity of sediment erosion in the nourished dry beach increases, the nourishment is weakened, and the recovery effect of the profile after the storm is not obvious. The results of the numerical modeling highlight that the dry beach nourishment method can resist storms to a certain extent, but the overall effect is relatively limited.

Key words: tropical storm, numerical model, XBeach, nourishment of dry beach, disaster mitigation efficiency

Citation: Zhao Yazhuang, Qi Hongshuai, Zhao Shaohua, Cai Feng, Liu Jianhui, Xu Pu, Xiao Zheyu, He Yanyu, Zhang Zhiyong. 2023. Nourishment and disaster mitigation efficiency of feeding sand on the dry section of a dissipative beach. Acta Oceanologica Sinica, 42(7): 138–148, doi: 10.1007/s13131-023-2193-7

1 Introduction

The coastline in China is tortuous and long and has abundant beach resources. From the perspective of beach morphodynamics, a parameter of "dimensionless fall velocity (Ω)" has been proposed, and beaches can be divided into reflective, dissipative and intermediate beaches (Wright and Short, 1984). Then, the scholars considered the impact of tides on beaches (Masselink and Short, 1993), which further expanded and supplemented the classification of beach types. Sandy beach resources along the coast of South China account for more than 1/3 of the total length of the coastline (Cai et al., 2005). These sandy beaches were shaped into different types by different hydrodynamics. A reflective beach has a steeper slope and narrower beach width and developed a dry beach (Yue et al., 2017); the fully dissipative beach is wide, gentle and flat, and the backshore often develops wind-produced landforms (Qi et al., 2009), while the features of the intermediate beach are moderate (Zhou et al., 2013). Different types of beaches have different morphological responses under the impact of storms. Based on 6 storm tracking surveys on 8 beaches in South China, Qi et al. (2009) discussed the different response patterns of beach morphology under the influence of storms on a completely dissipative beach and other types of beaches in South China. Ge et al. (2017) showed that there are differences in the storm response of beaches under different tidal ranges. Fiore et al. (2009) found that abnormal hydrodynamics generated by storms often cause severe damage to the backshore areas of beaches. Burvingt et al. (2017) found that in relatively sheltered bays, the impact of beach morphology is relatively small. Simultaneously, the evolution of beach morphology will continue to intensify as beaches suffer from storm clusters (Ferreira, 2005). Affected by human activities and changes in the environment, some near-shore beaches are seriously eroded. The nourishment of beaches has effectively mitigated beach erosion at home and abroad (Hanson et al., 2002; Song et al., 2005; Wang et al., 2009) and has resulted in significant economic income. As a common beach nourishment method, dry beach nourishment not only improves beach protection ability but also promotes the coastal tourism industry and protects communal facilities

Foundation item: The National Natural Science Foundation of China under contract No. 41930538; the Scientific Research Foundation of the Third Institute of Oceanography, Ministry of Natural Resources under contract No. 2022017.
*Corresponding author, E-mail: qihongshuai@tio.org.cn

(Zhuang et al., 2011; Cao et al., 2009). However, the nourished dry beach morphology will undergo a rapid adjustment process under both of normal and storm hydrodynamics (Liu et al., 2016; Dong et al., 2012).

Compared with other types of beaches, dry beaches don't exist at completely dissipative beaches under normal conditions, and when dry beaches are nourished at completely dissipative beaches, they are susceptible to impacts after a period of time, although they can reduce wave energy and protect against backshore erosion (Liu et al., 2016). The topographic evolution of the profile after beach nourishment has been studied extensively (Zhang, 2014; Xiao, 2021; Wang et al., 2020), but relatively little research has been done on the morphological evolution of the topography of fully dissipative beaches and the effects of storm energy dissipation on the nourishment of dry beaches. Beach storm response is a complex process that requires not only observations to analyze the beach response to storms and beach sediment transport patterns (Li et al., 2017; Zhu and Li, 2019; Su et al., 2019), but also numerical modeling to investigate the evolution of the beach. A series of analyses and verification experiments have been carried out by using the XBeach model, which shows that the model can simulate the response process of the beach profile well under the impact of storms, and the model has many applications in beach nourishment (Roelvink et al., 2009; Masselink et al., 2014; Zhu et al., 2019). This paper establishes the XBeach beach evolution model by observing the morphology and hydrodynamic data of Pingtan beach under the influence of Typhoon In-Fa, and use the measured data to verify the model. A series of numerical modeling experiments were carried out under normal and storm weather conditions to analyze the beach response patterns. Ultimately, the results enhance the understanding of the beach storm effect and provide ideas for coastal storm disaster prevention and mitigation.

2 Overview of the observation area

Pingtan Island is located in the western Taiwan Strait, and the observation area is located at Tianmei'ao Beach in Tannan Bay of Pingtan Island (referred to as TM beach) (Fig. 1). Affected by the monsoon circulation and the "funnel effect" of the Taiwan Strait, Pingtan Island has strong winds, with an average annual wind speed of 9.0 m/s and a maximum annual wind speed of 10.1 m/s. The wind direction is mostly SSW in summer and NNE in winter. Due to the influence of typhoons, from July to September, the wind peak speed occurs (Li, 2016b). The tidal types of the beach in the study area are regular semidiurnal tides; the maximum tidal range reaches 6.7 m, the minimum tidal range is 1.06 m, and the average tidal range is 4.25 m (He et al., 2018). The average significant wave height in the open sea is 1.1 m, the average period is 4.3 s to 7.3 s, and the coastal wave direction is ESE. TM beach is a completely dissipative beach, the slope of the intertidal zone is approximately 1/80, and the length is 2.3 km. The sediments on the beach are mainly coarse sand and medium sand, and the particle sizes is mainly range from 0.25 mm to 1.0 mm.

Typhoon In-Fa was generated in the western Pacific Ocean on July 18, 2021. It advanced to a typhoon at 14:00 on July 20 and became a strong typhoon at 11:00 on the 21st. After entering the East China Sea, it turned into a typhoon (Fig. 1). Typhoon In-Fa has a strong intensity and a wide range of impacts. During the observation period, the waves transmitted from the open sea to the nearshore were relatively high, and the observed water level changed greatly, which had an obvious impact on the TM beach in the study area.

3 Research methods

3.1 *Model building and validation*

XBeach (Reniers et al., 2009) is a plane-based two-dimensional coastal dynamic numerical model that is mainly used for

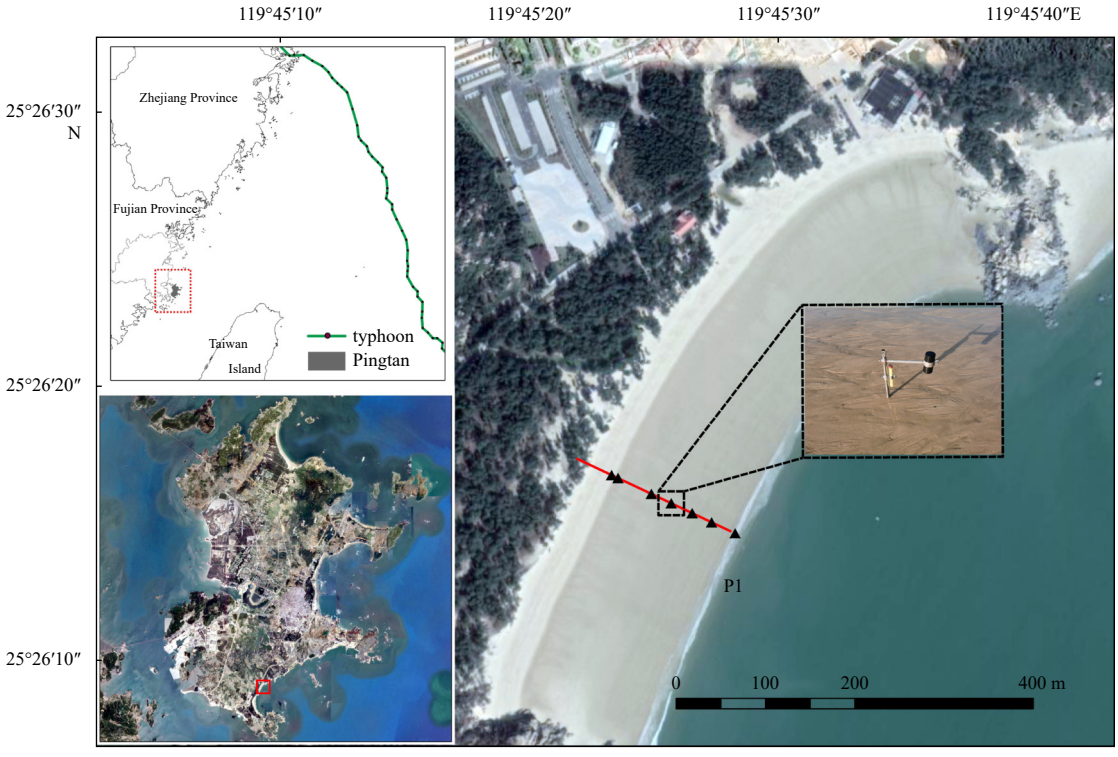

Fig. 1. Field observation position of the beach profile (the triangles mark the field observation positions).

simulation research on beaches. It uses a shallow-water equation averaged along the water depth to simulate low-frequency and wave-generated currents and uses the generalized Lagrangian average theory of the water depth average to simulate the water flow to the shore and the bottom reflux (Andrews and Mcintyre, 1978; Walstra et al., 2000). The wave energy balance equation is solved, considering wave refraction, shallow-water deformation, wave-current interaction and wave energy dissipation (Rienecker and Fenton, 1981; MacMahan et al.,2004); modes of bedrock and suspended transport are considered in the seabed profile evolution (Soulsby, 1997; Van Rijn, 2007), the sediment transport equation is used to solve the equilibrium concentration of sediment, and the water depth-averaged convection-diffusion equation is used to calculate the sediment concentration field (Li, 2016a). With continuous improvement and development of the model, the XBeach model has been able to simulate beach scour, dune (beach shoulder) erosion, overwashing, flooding and other storm response situations (Harley et al., 2011; Harter and Figlus, 2017).

This field observation was carried out at TM beach, Pingtan, from July 23 to July 28, 2021. Hydrodynamic observations along the cross-shore direction of the beach during Typhoon In-Fa were carried out (the field observation layout is shown in Fig. 2 below). Change in profile morphology were measured before and after the impact of the typhoon from July 23 to 25, which was used to verify the hydrodynamics and morphology of the XBeach model. RTK-GPS was used to repeatedly measure the changes in the beach profile. The RTK type is a STONEX S9 II PRO; its level and elevation accuracy are ±8 mm and ±15 mm, respectively; and the profile measurement range is from the toe of the backshore dune to the lower tide level. Simultaneously, 7 RBRsolo3D|wave16 wave tidal gauges were set up in the intertidal zone along the profile (Fig. 2). The sampling interval of wave-tide gauges is set as 5 min, and the sampling frequency is 4 Hz (Song et al., 2022).

As shown in Fig. 2, the XBeach numerical model in this paper is built from the wave gauge T1 set up at the farthest offshore distance from the P1 profile, with a model range of 0 m to 200 m, the grid size is 1 m. The model boundary adopts the tidal level and wave spectrum measured in the first 24 h as the boundary driving conditions (as shown in Fig. 3): the tidal level condition adopts the measured tide level data that changes every hour, and the wave uses the JONSWAP waveform data that changes every hour. The wave direction of the P1 profile is mainly vertical incidence (Zhu et al., 2019).

The morphological evolution model of the beach profile is verified based on the wave, tide level and profile morphology data observed in the field. The XBeach model takes the actual topography of the first P1 profile (Fig. 1) as the initial topographic condition and uses the topographic data of the P1 profile measured after 24 h to verify the parameters of the numerical model. Instruments T2–T7 on the P1 section (Fig. 2) are verified by the measured wave data (Song et al., 2022). The wave changes are shown in Fig. 4. The wave data measured by instruments T2–T7 are selected for verification. The results show that the Pearson correlation coefficients between the simulated wave height of the instrument arranged on the P1 section and the measured wave

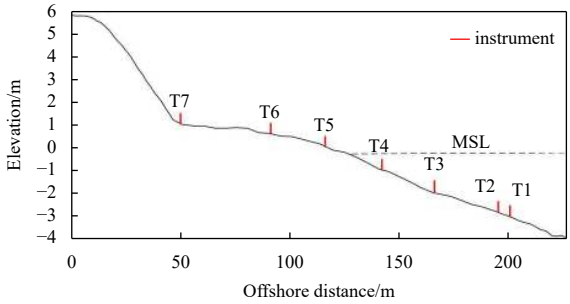

Fig. 2. Profile of observation and instrument layout. MSL: mean sea level.

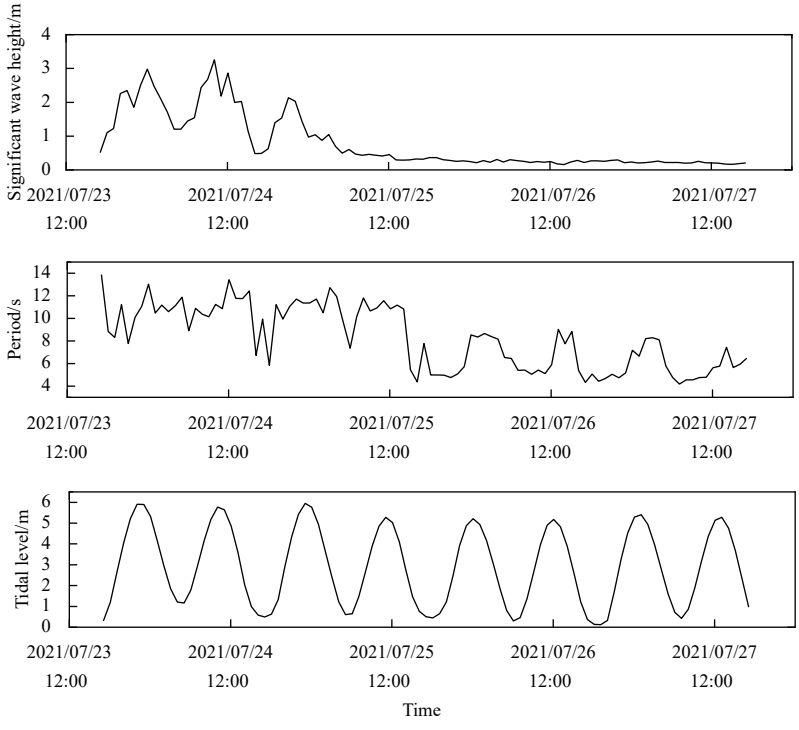

Fig. 3. Measured boundary driving conditions.

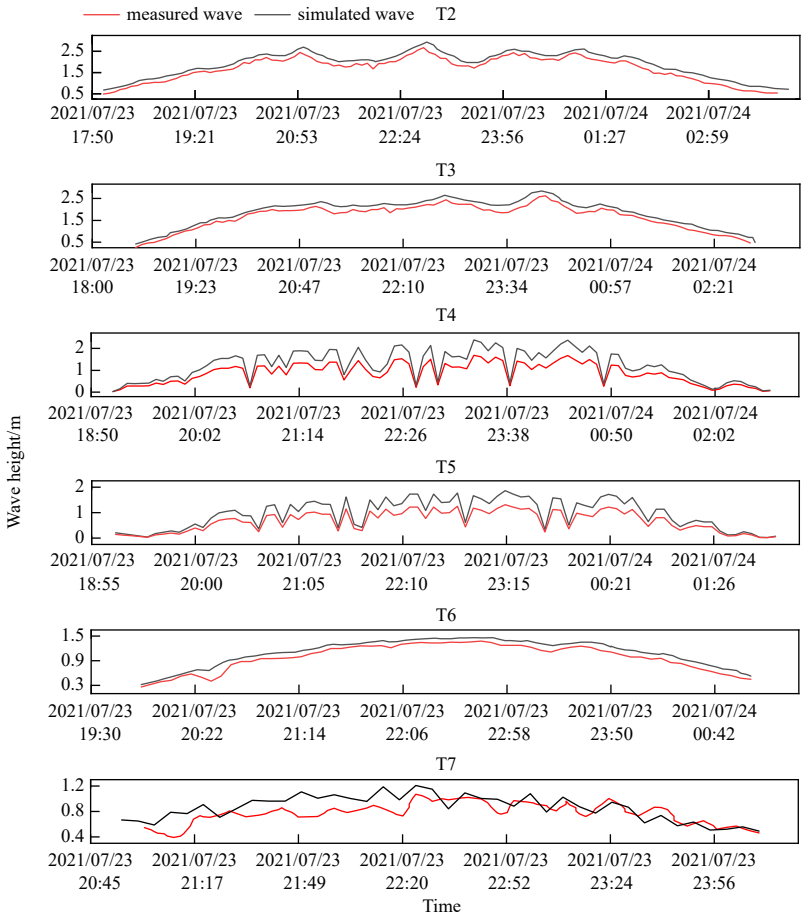

Fig. 4. Wave verification at different sites.

height are all greater than 0.7, and the results are credible.

To verify the accuracy of the XBeach numerical model to simulate the profile morphology, the Brier Skill Score (BSS) empirical coefficient was used to evaluate the rationality of the beach terrain simulation and to analyze the sensitivity of parameters such as facua (Liang et al., 2021; Li, 2017). The BSS evaluation method is widely used in evaluations of the dynamic simulation of coastal geomorphology. Values ranging from 1.0 to 0.5 are excellent, 0.5 to 0.2 are good, 0.2 to 0.1 are reasonable, 0.1 to 0.0 are bad, and <0.0 are poor. The BSS is calculated using the following formula,

$$\mathrm{BSS} = 1 - \frac{\mathrm{MSE}(Y,X)}{\mathrm{MSE}(B,X)}, \tag{1}$$

$$\mathrm{MSE}\,(Y,X) = \frac{1}{J}\sum_{i=1}^{j}(y_i - x_i)^2. \tag{2}$$

In the formula, parameter B represents the initial profile topography data, X represents the measured profile topography after 24 h of simulation, and Y represents the profile morphology simulated by the XBeach model (Fig. 5). The profile morphology and the corresponding BSS value under different parameter values are calculated. The corresponding BBS value is 0.863. Thus the simulated topography agrees with the measured P1 profile topography, indicating that the XBeach model established in this paper can describe the actual beach topography change well.

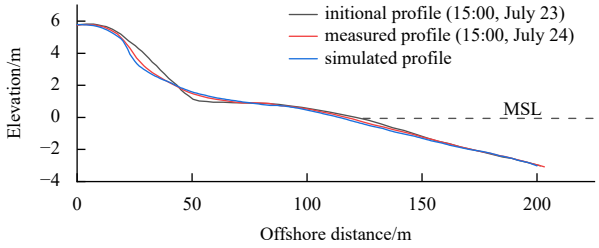

Fig. 5. Verification of the profile morphology. MSL: mean sea level.

3.2 *Model settings*

In this paper, we mainly simulate the dry beach profiles for different profile arrangements of nourishment sizes and nourished sand volume per unit width, which were set to nourish dry beach sizes of 20 m, 40 m, and 80 m (Gong, 2019; Fan, 2018), and nourished sand volume per unit width of 7.86 m^3/m, 26.11 m^3/m, and 79.3 m^3/m, respectively (Fig. 6). Considering the effect of different nourished sand volume per unit width, the nourished sand volume per unit width increases to 174 m^3/m on the basis of the initial size of an 80 m dry beach alone (Fig. 7). The sediment size is 0.368 mm, and the slope is designed according to 1:10, which is consistent with the slope design of the beach nourished project. The dynamic conditions under normal weather and different storm conditions are simulated separately, where H_0 and H_2 represent normal weather conditions with no water enhancement effect, while S_1, S_2 and S_3 represent different degrees of storm

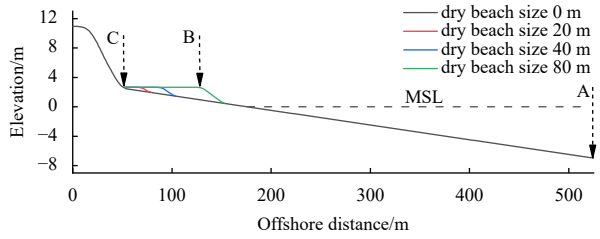

Fig. 6. Morphology of nourished profiles with different dry beach sizes (Point A is the boundary of the model, Point B is the outer edge of the dry beach shoulder of the nourished profile, and Point C is the toe of the backshore). MSL: mean sea level.

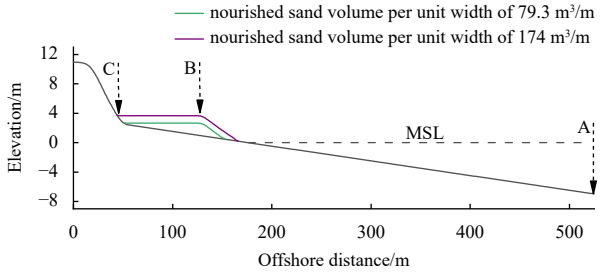

Fig. 7. Topography of nourishment profiles with different nourished sand volumes per unit width (Point A is the boundary of the model, Point B is the outer edge of the dry beach shoulder of the nourished profile, and Point C is the toe of the backshore). MSL: mean sea level.

conditions with different degrees of water enhancement, and the specific working conditions are shown in Table 1.

4 Analysis of model results

4.1 *Results of beach evolution after dry beach nourishment*

During the long-term evolution of the nourished dry beach under normal weather conditions, the degree of dry beach erosion gradually increases, its morphology is destroyed, a large amount of sediment is lost from the dry beach, and some sediment is carried to accumulate above the dry beach (Figs 8a, b). Under the action of H_0W_3 and H_0W_4 conditions for a long time (as shown in Table 1, H_0W_3 and H_0W_4 conditions indicate that the ocean hydrodynamic force under normal weather conditions continues to act on the dry beach profile with different nourished sand volume per unit width for 90 days), the nourished dry beach profile suffers certain changes of washout and siltation, the ocean hydrodynamic force crosses the dry beach, the nourished dry beach is eroded landward, part of the eroded beach sand is carried to accumulate above the dry beach (Fig. 8a), the maximum accumulation thickness is 0.55 m, the slope form of the dry beach is changed, and the maximum erosion thickness of the nourished dry beach is 1.15 m (Fig. 8c). As the nourished sand volume per unit width of the nourished dry beach increases, the degree of erosion of the dry beach increases under the influence of ocean hydrodynamics and the gravity of the dry beach itself, and the maximum erosion thickness of the nourished dry beach is 1.53 m. The eroded beach sand is transported offshore and accumulates in the lower beach surface with a convex accumulation of 0.88 m (Fig. 8c).

4.2 *Simulation results for a nourished beach under storm conditions*

4.2.1 *Simulation results of nourishment profiles with different dry beach sizes*

Under the extreme hydrodynamic impact of the storm, with sediment erosion on the slope above the beach backshore under extreme storm hydrodynamics, and the degree of sediment erosion increases with increasing storm action. Under the impact of a weak storm, sediment erosion and deposition changes are relatively small, and dry beach morphology is preserved, whereas under stronger storms, the morphological response of the nourished dry beach increases, and the sediment migrates offshore. The lower beach surface is eroded to different degrees, and the eroded sediment migrates offshore. The sediment eroded with different dry beach widths is deposited at almost the same location on the lower beach, and the sediment deposition thickness is basically the same (Fig. 8).

Under storm condition S_1, the thickness of sediment erosion and deposition along the nourished profile varies for different dry beach widths (Figs 9a, d). When the size of the nourished dry beach is 20 m, the maximum erosion thickness of the backshore slope is 0.97 m. As the size of the nourished dry beach increases, the erosion degree decreases. At this time, the maximum erosion thicknesses of the backshore slope are 0.92 m and 0.80 m, and the eroded sediment is deposited at the bottom of the slope above the backshore. The nourished dry beaches of different sizes are all eroded under the impact of the storm, and the maximum erosion thicknesses of the sediment are 0.15 m, 0.54 m, and 0.61 m. The eroded sediment is deposited at the bottom of the slope above the nourished dry beach.

Under storm condition S_2, the sediment erosion along the nourished profile of different dry beach sizes is similar to the former (Figs 9b, e). For the nourished dry beach size of 20 m, under the impact of S_2, the maximum erosion thickness on the backshore slope is 1.33 m. When the sizes of the nourished dry beach are 40 m and 80 m, the maximum erosion thicknesses of the backshore slope are 1.27 m and 1.23 m, and the maximum erosion thicknesses of the nourished dry beach are 0.56 m and 0.62 m, which are not much different from the effect of working condition S_1. The sediment deposition at the bottom of the slope in front of the nourished dry beach decreases, and the sediment

Table 1. Numerical simulation conditions

Conditions	Maximum significant wave height/m	Maximum increase water/m	W_1	W_2	W_3	W_4
			20 m (7.86 m³/m)	40 m (26.11 m³/m)	80 m (79.3 m³/m)	80 m (174 m³/m)
H_0	0.8	0	–	–	90 d	90 d
S_1	3.5	1.0	72 h	72 h	72 h	–
S_2	4.5	1.5	72 h	72 h	72 h	72 h
S_3	5.5	2.0	72 h	72 h	72 h	–
H_2	0.8	0	–	–	30 d	30 d

Note: The significant wave height and storm water increase are both time series changes. – represents no data.

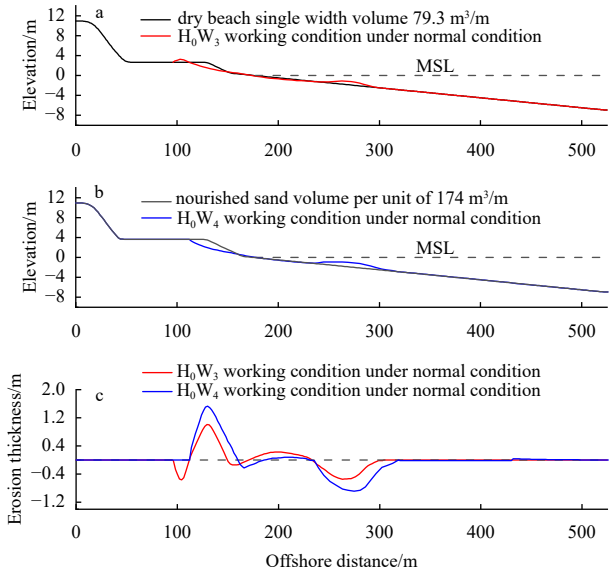

Fig. 8. Simulation results of different nourished sand volume per unit width profiles and sediment erosion thickness along the course under the action of H_0W_3 and H_0W_4 working conditions.

deposition position on the lower beach migrates forward and increases. Subsequently, the beach sediment is in a state of erosion.

Compared with S_1 and S_2, under the storm condition S3, the response degree of the nourished profiles with different dry beach sizes is the largest (Figs 9c, f). At this time, the maximum sediment erosion thicknesses of the slope above the backshore are 1.89 m, 1.81 m and 1.68 m, and the sediment deposition at the bottom of the slope increases. When the nourished dry beach size is 20 m, the nourished dry beach sediment is less affected. When the nourished dry beach sizes are 40 m and 80 m, the maximum erosion thicknesses of the dry beach are 0.57 m and 1.12 m, respectively. There is more sediment erosion on the beach surface below the dry beach. Some eroded sediment deposits on the beach surface and the sediment at the boundary of the beach are slightly eroded.

4.2.2 *Simulation results of nourishment profiles with different nourished sand volume per unit width*

For the nourishment effect of different nourished sand volume per unit width profiles, this section mainly uses S_2 storm conditions for simulation analysis. Under the strong storm ocean hydrodynamic action, for the profile with a small nourished sand volume per unit width, under the combined action of storm water and storm waves, the seawater can easily cross the nourished dry beach, forming a more obvious diffuse beach process and causing making the backshore slope sediment erosion with a maximum erosion thickness of 1.23 m and nourished dry beach landward erosion (Figs 10a, c). As the nourished sand volume of the nourished dry beach increases, the storm hydrodynamic force is consumed more at the location of the front slope of the nourished dry beach, the seawater slightly crosses the dry beach, and a small amount of sediment accumulates in the upper part of the dry beach, and the maximum erosion thickness of the nourished dry beach is 1.28 m at this time (Figs 10b, c).

4.3 *Simulation results of beach evolution after storms*

In the fully dissipative beach profile after the storm, under normal weather conditions, the sediment migrates in part of the

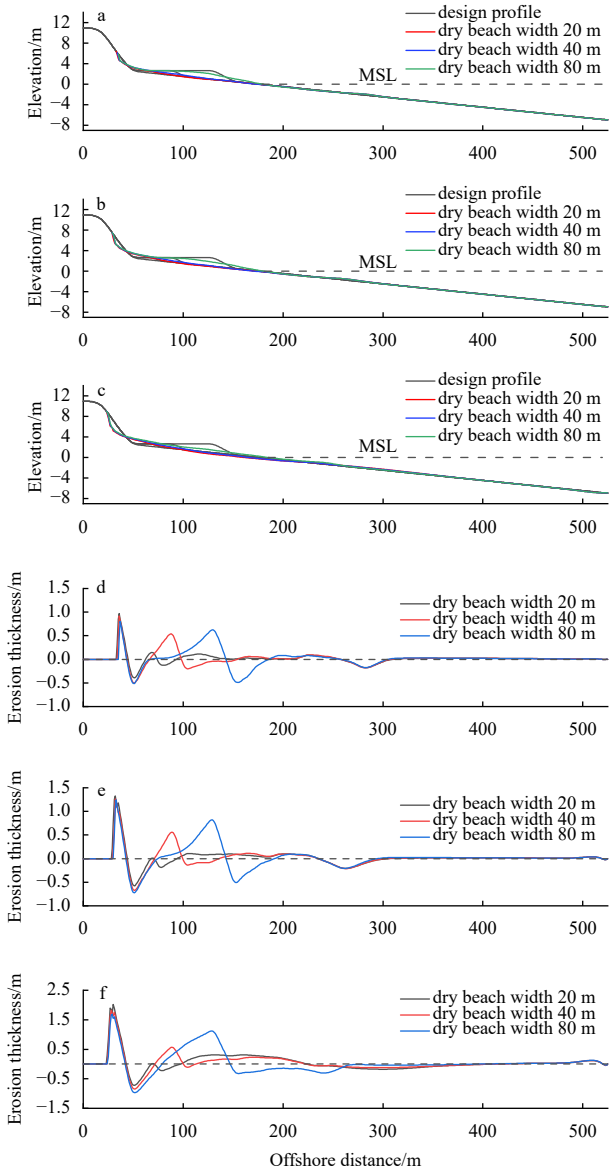

Fig. 9. Simulation results of the nourished dry beach profile and the thickness of sediment intrusion along the profile route under different working conditions. Simulation results of S_1W_1, S_1W_2 and S_1W_3 working conditions (a, d); simulation results of S_2W_1, S_2W_2 and S_2W_3 working conditions (b, e); simulation results of S_3W_1, S_3W_2 and S_3W_3 working conditions (c, f).

beach profile, and the overall evolution degree of the profile is small. At this time, the beach profile recovery after the storm is not obvious (Fig. 11). Under the H_2W_3 working condition, the overall response of the storm profile is small, and the sediment at the dry beach continues to erode. Compared with the storm profile, the maximum erosion thickness increases by 0.22 m, and part of the eroded sediment is alluvial in the upper part of the dry beach. The maximum deposition thickness is 0.18 m (Figs 11a, c). Compared to the nourishment profile with a larger nourished sand volume per unit width, the entire storm profile responds to a lesser extent under the action of working condition H_2W_4, with almost no change in the beach profile and a small amount of sediment transported slightly offshore by ocean hydrodynamics (Figs 11b, d). In general, after the storm, the storm profile recovers under normal wave conditions, while for fully dissipated

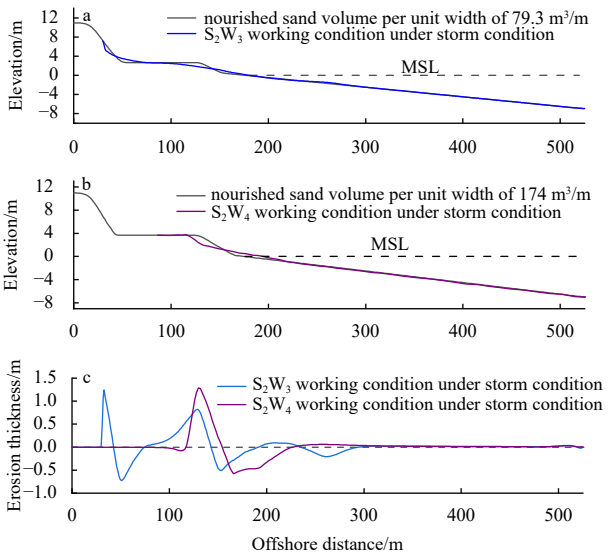

Fig. 10. Simulation results of profiles with nourished sand volume per unit width and sediment erosion thickness along the course under the action of S_2 storm conditions.

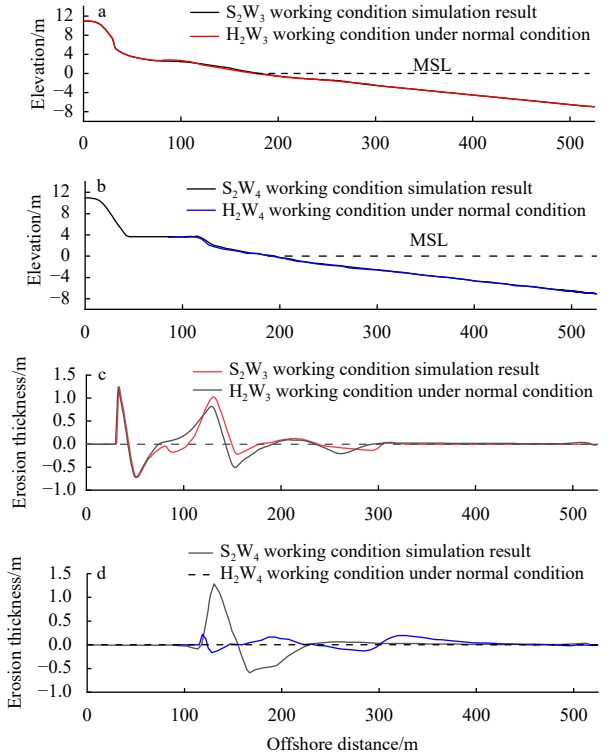

Fig. 11. Simulation results of storm profiles and sediment erosion thickness of dry beaches with different nourished sand volume per unit width. Simulation results of S_2W_3 and H_2W_3 conditions (a, c); simulation results of S_2W_4 and H_2W_4 conditions (b, d). MSL: mean sea level.

beaches, after a period of recovery, the recovery effect is less obvious, the dry beach morphology recovers less, the overall sediment is in an erosion state, the beach profile morphology is basically unchanged, and the beach sediment is still in a deficit state compared with the initial nourishment of the dry beach profile.

5 Discussion

5.1 *Storm response of nourished dry beaches with different profile arrangements*

There are significant differences in the responses of different profile arrangements of nourished dry beach profiles under storm action, and the change in the profile (MPC) is introduced here to explore the degree of change in beach migration under storm action for different profile arrangements of nourished dry beach profiles (Qi et al., 2010).

$$\mathrm{MPC} = \int_{x_0}^{x_1} |z_a - z_b| \, \mathrm{d}x, \tag{3}$$

$$\omega = \frac{\mathrm{MPC}}{\Delta t \times (x_0 - x_1)}, \tag{4}$$

where z_a and z_b represent the initial profile before the storm action and the beach profile elevation after the storm action, $x_0 - x_1$ represents the total beach length, ω represents the rate of change of beach migration, and Δt represents the time of storm action. The calculated rates of change in migration of different profile arrangements of nourished dry beach profiles are shown in Table 2.

When dry beach nourishment is finished on a fully dissipative beach, storm waves start to dissipate on the lower beach surface and on the dry beach. At this time, the dry beach sediment is easily eroded and carried by seawater and deposited in different locations. There are differences in beach storm responses under different storm conditions. When there is a stronger storm in-

Table 2. Rates of changes in the migration of different profile arrangements of nourished dry beach profiles under the effect of storms

Numerical simulation conditions	Different profile arrangement of nourished dry beaches	Rates of changes in the migration of nourished dry beach profiles (ω)
S_1	20 m (7.86 m³/m)	0.017
	40 m (26.1 m³/m)	0.024
	80 m (79.3 m³/m)	0.032
S_2	20 m (7.86 m³/m)	0.027
	40 m (26.1 m³/m)	0.032
	80 m (79.3 m³/m)	0.043
	80 m (174 m³/m)	0.036
S_3	20 m (7.86 m³/m)	0.055
	40 m (26.1 m³/m)	0.061
	80 m (79.3 m³/m)	0.072

Table 3. Characteristic values of the variations in intrusion and silting variation in nourished dry beaches of different sizes

Numerical simulation conditions	Dry beach size/m	Amount of change per unit width/m³	Dry beach erosion distance/m
S_1	20	26.8	7
	40	37.8	23
	80	50.4	36
S_2	20	42.5	0
	40	50.4	18
	80	67.7	42
S_3	20	86.6	0
	40	96.1	18
	80	113.4	51

tensity and larger storm wave, the change in the beach morphology increases. For a nourished dry beach in a completely dissipative beach, during the storm impact, it carries more consumptive wave energy, which is often greatly affected. Based on Tables 2 and 3, it is given that there is a difference in the degree of the response of different nourished dry beach size profiles under storm action, the stronger the storm action is, the greater the increase in the beach migration rate and erosion degree of different widths of nourished dry beach profiles, while the average amount of change in beach profiles increases gradually as the dry beach size increases under the same storm action. Increasing the nourished sand volume of the nourished dry beach, the dry beach has sufficient sand source, and the erosion of the nourished dry beach increases under the influence of continuous storm hydrodynamic force and the self-weight of the dry beach (Table 3), Fig. 10b shows that the beach backshore is basically unaffected, and the overall migration rate of the beach at this time is slightly lower than that of the nourishment profile with a small nourished sand volume (Table 2).

Dry beach nourishment sizes have a significant effect on the degree of beach storm response, providing an abundant source of erodible sand during storm action when the nourished dry beach is wider and larger in size, thereby enhancing the beach defenses to some extent (Liang et al., 2021). In contrast, under extreme storm conditions, there is also dry beach sand loss. For the storm response characteristics of fully dissipative beaches, when the sand source on the beach is more abundant, the storm wave energy is more fully dissipated on the dry beach, and the degree of its storm response is more significant (Table 3).

5.2 *Analysis of energy consumption for nourished dry beaches with different profile arrangements*

The model results show that the storm response degree of the nourished dry beach with different sizes and nourished sand volume per unit width are also different. With the increase in the dry beach sizes and nourished sand volume per unit width, the nourished dry beach is eroded. Erosion continues to increase and the morphology of the nourished dry beach changes. From the perspective of dynamics, waves are the main controlling factor affecting the evolution of dry beach. Therefore, it is necessary to further analyze the wave weakening ability and disaster reduction efficiency of nourished dry beaches with different widths under the impact of storms.

The wave height attenuation rate (R_{wl}) refers to the wave height H_0 in the process of shore propagation, passing through the beach of width L. Then, the ratio of the wave height attenuation (H_0–H_L) to the original wave height H_0 is calculated according to the following formula (Qi et al., 2020),

$$R_{wl} = \frac{H_0 - H_L}{H_0} \times 100\%, \tag{5}$$

where H_0 and H_L are the wave height inside the wave breaking zone and the wave height outside the wave breaking zone, respectively, and the units are m.

Under different storm intensity conditions, the wave energy attenuation rates from the outer edge of the dry beach shoulder (Point B) to the bottom of the backshore slope (Point C) were calculated respectively (Fig. 6). The energy dissipation effect of different profile arrangements of nourished dry beaches under the impact of storms was studied through comparative analysis, and when combined with the wave difference at Points B and C of different profile arrangements of nourished dry beaches, the disaster reduction efficiency of nourished dry beaches is discussed.

Under different storm conditions, from Point B on the outer edge of the beach shoulder to Point C at the bottom of the backshore section, the wave attenuation rates of the nourished dry beach are different (Table 4). The wave attenuation rate from Point B to Point C on the outer edge of the dry beach shoulder increases and the dissipation process is more significant when the nourished sizes of the dry beach increase with the same intensity of storm action (Table 4). This relationship occurs because when the beach profile is subjected to storm impact, the wider the nourished dry beach is, the less wave energy is consumed on the beach between the bottom of the dry beach slope and the model boundary. When the storm wave reaches the slope of the nourished dry beach, more wave energy is dissipated. As the size of the nourished dry beach increases, the storm waves acting on the dry beach become stronger, and more storm wave energy is consumed as the storm waves interact with the nourished dry beach. When the size of the nourished dry beach is constant, the smaller the intensity of the storm action is, the greater the wave attenuation rate from Point B of the nourished dry beach to Point C of the backshore, and the wave mitigation effect is more obvious (Table 4).

As the nourished sand volume per unit width of the nourished dry beach increases, the degree of energy consumption of the nourished dry beach storm increases. Compared with the nourished sand volume per unit width of the small profile, the difference in the degree of energy consumption of the beach below the dry beach at this time is not significant. With the action of storm waves on the dry beach, the greater the nourished sand volume per unit width, the more abundant the sand source and the relative increase in storm waves and the degree of action of the dry beach, so the degree of energy consumption of the dry beach increases (Table 4).

During a storm, the storm waves are dissipated on the beach surface. Under the same storm conditions, when the storm waves are not interacting with the nourished dry beach, there is little variation in the attenuation rate of the wave height along the beach surface below the dry beach. When the storm wave interacts with the nourished dry beach, the degree of wave dissipation increases. As the nourished dry beach size and nourished sand volume per unit width increase, the degree of wave dissipation increases and its wave attenuation rate increases. As the storm waves interact with the nourished dry beach, the nourished dry beach has a certain wave dissipation effect, and the degree of storm wave attenuation is enhanced. Compared with weak storms, the nourished dry beach has a weaker effect on wave dissipation during stronger storms (Fig. 12).

5.3 *Evolution model of a fully dissipative beach after dry beach nourishment*

The fully dissipative beach has a relatively wide and flat sur-

Table 4. Characteristic values of wave attenuation rates for different profile arrangements of nourished dry beach profiles

Different profile arrangements of nourished dry beaches		B to C wave height attenuation rate/%		
		S_1	S_2	S_3
Dry beach size/m	20	52	37	32
	40	67	49	42
	80	72	56	54
Nourished sand volume per unit width/($m^3 \cdot m^{-1}$)	79.3	–	56	–
	174	–	62	–

Note: – represents no data.

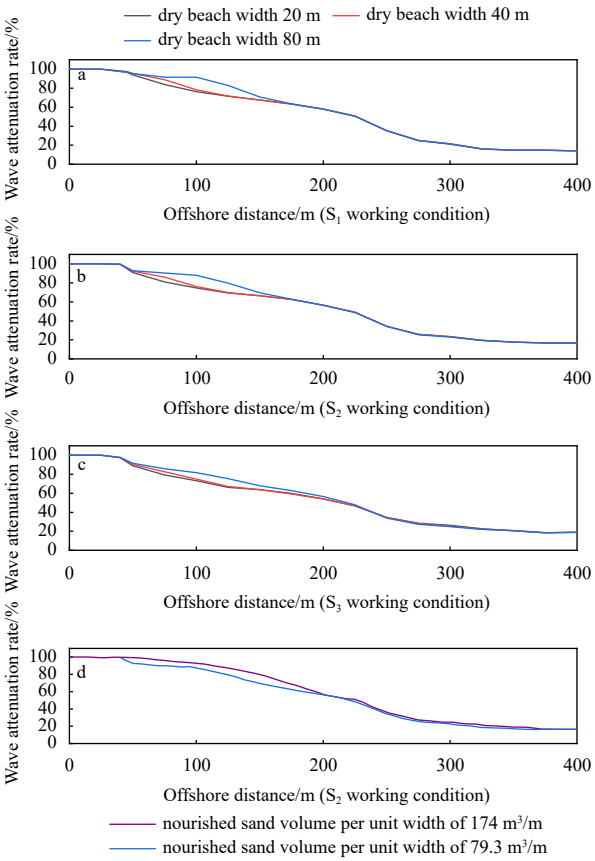

Fig. 12. Variation in the wave attenuation rate for different profile arrangements of nourished dry beach profiles. Wave energy dissipation for different dry beach size nourishment profiles (a–c); wave energy dissipation for different nourished sand volume profiles (d).

face, and the waves generated under normal weather and during storms are largely dissipated on the beach surface. After analyzing the nourished effect of the fully dissipative dry beach, under the normal hydrodynamic action of H_0W_3 and H_0W_4 conditions for a long time, the response of the beach profile is larger, the amount of sediment erosion of the nourished dry beach gradually increases, the local erosion of the beach surface deepens, some sediment is lost, and the morphology of the nourished dry beach is damaged (Figs 13a, c and 14a). After the short-term effect of the storm, the existence of the nourished dry beach can play an important role in reducing waves and in protection and disaster reduction for the backshore, which is mainly realized by redistribution of sediment erosion in the beach system and the dynamic adjustment of the dry beach (Fig. 14b). After the storm, under normal weather conditions, the nourished dry beaches showed a certain recovery trend, but the recovery effect is not obvious (Figs 13b, d and 14c). Therefore, although dry beach nourishment on fully dissipative beaches can protect the backshore, the nourished dry beach effect is slightly worse, and the nourishment of dry beach sand can be easily lost and not easily recovered.

6 Conclusions

In this paper, based on the topographic and hydrodynamic data of typical fully dissipative beach profiles measured in the field, an XBeach numerical model is established to verify the profile elevation evolution model of Pingtan TM beach under the influence of Typhoon In-Fa. Based on the analysis of the pattern of different widths on nourished dry beaches in dissipative beaches under normal and storm weather conditions, the nourished effect and disaster mitigation efficiency of dry beaches are discussed, and the following conclusions are obtained.

(1) The morphology of the profile changes with different storm hydrodynamic conditions of the storm. The stronger the

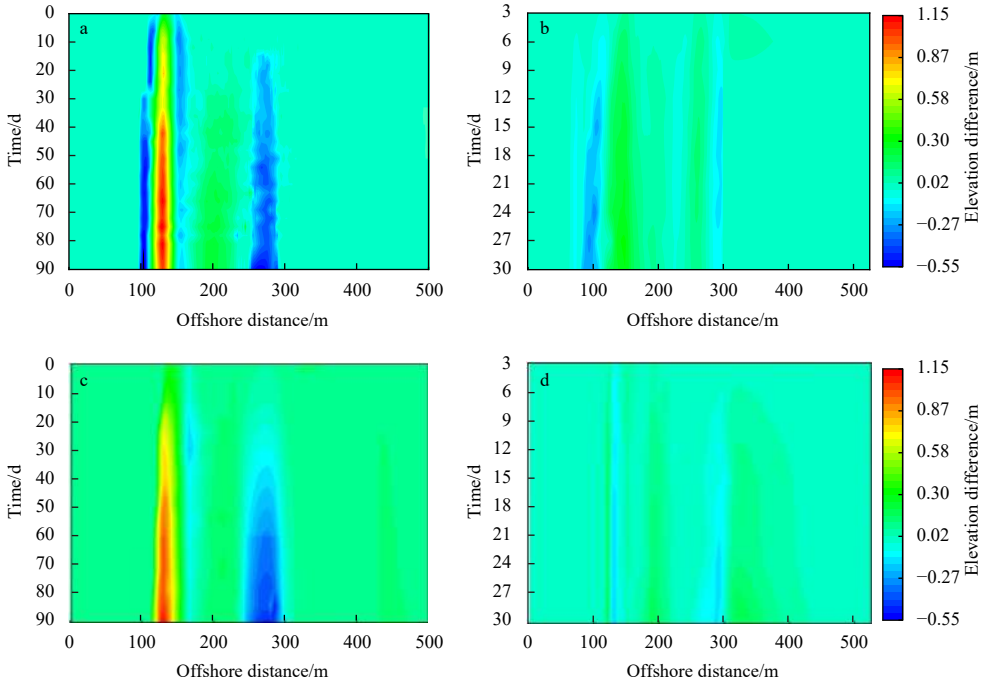

Fig. 13. Long-term evolution of the initial profile and the storm beach profile under normal weather conditions. Evolution of the profile with a nourished sand volume per unit width of 79.3 m³/m (a, b); evolution of the profile with a nourished sand volume per unit width of 174 m³/m (c, d).

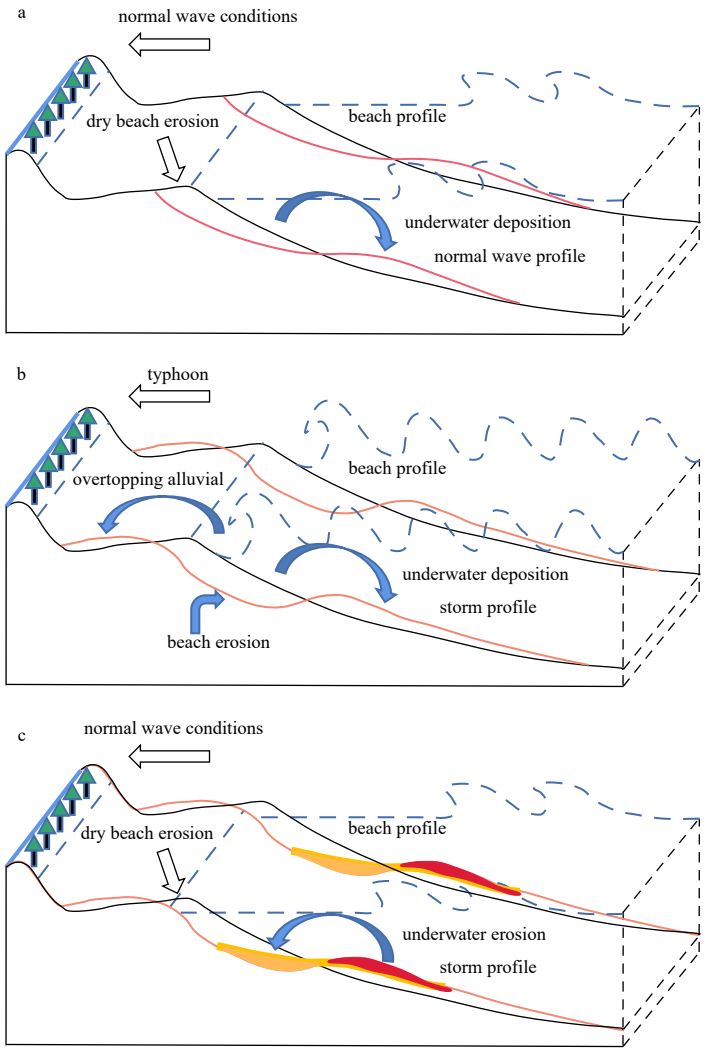

Fig. 14. Evolution of a fully dissipative dry beach under different conditions after nourishment.

storm is, the greater the dry beach response and the more sediment loss that occurs, while at the same storm intensity, as the dry beach size increases, the beach surface consumes less storm energy, and the degree of nourished dry beach response increases.

(2) The existence of the nourished dry beach in front of the beach efficiently mitigates wave energy. Under the same storm conditions, as the size and nourished sand volume per unit width of the nourished dry beach increases, the wave height attenuation rate of the nourished dry beach increases. As the waves increase under the effect of stronger storms, the wave height attenuation rate of the same size of the nourished dry beach decreases, and at this time, when the intensity of the storm is smaller, the effect of the nourishment dry beach wave elimination is more obvious.

(3) The existence of nourished dry beach plays a certain protection and disaster mitigation role in the backshore, but the dry beach sediment is subject to much erosion, weakening the stability of the dry beach. After a storm under the action of normal waves, although the nourished dry beach has been restored, the effect is less obvious. From the model results.The model results reveal that fully dissipative beaches are less suitable for dry beach nourishment, with easy loss of beach sand and poor recovery ability; this finding has reference value, but should be analyzed in conjunction with beach monitoring data to fully explain the effect of dry beach nourishment for fully dissipative beaches.

References

Andrews D G, Mcintyre M E. 1978. An exact theory of nonlinear waves on a Lagrangian-Mean flow. Journal of Fluid Mechanics, 89(4): 609–646, doi: 10.1017/S0022112078002773

Burvingt O, Masselink G, Russell P, et al. 2017. Classification of beach response to extreme storms. Geomorphology, 295: 722–737, doi: 10.1016/j.geomorph.2017.07.022

Cai Feng, Su Xianze, Cao Huimei, et al. 2005. Analysis on morphodynamics of sandy beaches in South China. Haiyang Xuebao (in Chinese), 27(2): 106–114

Cao Huimei, Cai Feng, Chen Feng. 2009. The conservation of coastal beaches and development of marine tourism of Xiamen City. Ocean Development and Management (in Chinese), 26(7): 58–62

Dong Lihong, Liang Shuxiu, Sun Zhaochen. 2012. Progress on beach nourishment theory and experimental researches. Ocean Development and Management (in Chinese), 29(5): 44–51

Fan Rongshan. 2018. Numerical investigation of the erosion of coastal sand dune (in Chinese)[dissertation]. Dalian: Dalian University of Technology

Ferreira Ó. 2005. Storm groups versus extreme single storms: predicted erosion and management consequences. Journal of Coastal Research, 42: 221–227

Fiore M M E, D'Onofrio E E, Pousa J L, et al. 2009. Storm surges and

coastal impacts at Mar Del Plata, Argentina. Continental Shelf Research, 29(14): 1643–1649, doi: 10.1016/j.csr.2009.05.004

Ge Zhenpeng, Dai Zhijun, Pang Wenhong, et al. 2017. LIDAR-based detection of the post-typhoon recovery of a meso-macro-tidal beach in the Beibu Gulf, China. Marine Geology, 391: 127–143, doi: 10.1016/j.margeo.2017.08.008

Gong Yumeng. 2019. Research on restoration of muddy sand beach (in Chinese)[dissertation]. Hangzhou: Zhejiang University

Hanson H, Brampton A, Capobianco M, et al. 2002. Beach nourishment projects, practices, and objectives—a European overview. Coastal Engineering, 47(2): 81–111, doi: 10.1016/S0378-3839(02)00122-9

Harley M, Armaroli C, Ciavola P. 2011. Evaluation of XBeach predictions for a real-time warning system in Emilia-Romagna, Northern Italy. Journal of Coastal Research, 64: 1861–1865

Harter C, Figlus J. 2017. Numerical modeling of the morphodynamic response of a low-lying barrier island beach and foredune system inundated during Hurricane Ike using XBeach and CSHORE. Coastal Engineering, 120: 64–74, doi: 10.1016/j.coastaleng.2016.11.005

He Yanyu, Liu Jianhui, Cai Feng, et al. 2018. Progress of research on Aeolian sediment transport influenced by tide. Journal of Desert Research (in Chinese), 38(3): 455–463

Li Wenshan. 2016a. Numerical research on beach and dune evolution under storm conditions (in Chinese)[dissertation]. Tianjin: Tianjin University

Li Songqiao. 2016b. Numerical simulation of wind waves and storm surges in Pingtan Bay (in Chinese)[dissertation]. Tianjin: Tianjin University

Li Rui. 2017. Numerical simulation of sandy beach profile response to storm surge in Xiamen Island (in Chinese)[dissertation]. Nanjing: Southeast University

Li Shushi, Dai Zhijun, Ge Zhenpeng, et al. 2017. Sediment dynamic processes of macro-tidal beach in response to Typhoon Rammasun action—A case study of Yintan, Beihai. The Ocean Engineering (in Chinese), 35(3): 89–98

Liang Bingchen, Zhu Meixi, Qu Zhipeng, et al. 2021. Comparative analysis on numerical simulation of the impacts of different beach nourishment schemes on beach profile. Haiyang Xuebao (in Chinese), 43(11): 136–145

Liu Jianhui, Cai Feng, Li Boliang, et al. 2016. Effect of Beach Nourishment on the Coastal Aeolian Sand Accumulation: a case study in Pingtan, Fujian, China. Journal of Desert Research (in Chinese), 36(3): 565–574

MacMahan J H, Reniers A J H M, Thornton E B, et al. 2004. Infragravity rip current pulsations. Journal of Geophysical Research: Oceans, 109(C1): C01033

Masselink G, McCall R, Poate T, et al. 2014. Modelling storm response on gravel beaches using XBeach-G. Proceedings of the Institution of Civil Engineers-Maritime Engineering, 167(4): 173–191, doi: 10.1680/maen.14.00020

Masselink G, Short A D. 1993. The effect of tide range on beach morphodynamics and morphology: A conceptual beach model. Journal of Coastal Research, 9(3): 785–800

Qi Hongshuai, Cai Feng, Lei Gang, et al. 2009. Study on storm response characteristics of south China beach. Progress in Natural Sciences (in Chinese), 19(9): 975–985

Qi Hongshuai, Cai Feng, Lei Gang, et al. 2010. The response of three main beach types to tropical storms in South China. Marine Geology, 275(1–4): 244–254

Qi Hongshuai, Cai Feng, Yu Fan, et al. 2020. T/CAOE 21.7-2020 Technical guideline on coastal ecological rehabilitation for hazard mitigation—Part 7: Sandy coast (in Chinese). Beijing: China Association of Oceanic Engineering

Reniers A J H M, MacMahan J H, Thornton E B, et al. 2009. Surf zone surface retention on a rip-channeled beach. Journal of Geophysical Research, 114(C10): C10010, doi: 10.1029/2008JC005153

Rienecker M M, Fenton J D. 1981. A Fourier approximation method for steady water waves. Journal of Fluid Mechanics, 104: 119–137, doi: 10.1017/S0022112081002851

Roelvink D, Reniers A, van Dongeren A, et al. 2009. Modelling storm impacts on beaches, dunes and barrier islands. Coastal Engineering, 56(11–12): 1133–1152

Song Xiangqun, Guo Zijian, Chen Shiyin. 2005. The planning and design of artificial beach in the Xinghai Bay. China Civil Engineering Journal (in Chinese), 38(4): 134–140

Song Jiacheng, Qi Hongshuai, Zhang Chi, et al. 2022. Analysis of energy dissipation process of wave propagation in beach foreshore under the influence of tide. Journal of Tropical Oceanography (in Chinese), 41(4): 146–153

Soulsby R L. 1997. Dynamics of Marine Sands: A Manual for Practical Applications. London: Thomas Telford

Su Fangfang, Cai Feng, Qi Hongshuai, et al. 2019. Study on various response to typhoon of nourished beaches with different sediments. Haiyang Xuebao (in Chinese), 41(7): 103–115

Van Rijn L C. 2007. Unified view of sediment transport by currents and waves. I: Initiation of motion, bed roughness, and bed-load transport. Journal of Hydraulic Engineering, 133(6): 649–667, doi: 10.1061/(ASCE)0733-9429(2007)133:6(649)

Walstra D J R, Roelvink J A, Groeneweg J. 2000. Calculation of wave-driven currents in a 3D mean flow model. In: 27th International Conference on Coastal Engineering. Sydney: American Society of Civil Engineers, 1050–1063

Wang Ganglu, Cai Feng, Cao Huimei, et al. 2009. Study on the practice and theory of beach replenishment of Xiangshan-Changweijiao Beach in Xiamen. Ocean Engineering (in Chinese), 27(3): 66–75

Wang Cong, Liang Bingchen, Wang Jun, et al. 2020. Experimental study on beach nourishment with sand filling. China Water Transport (in Chinese), 20(10): 147–149

Wright L D, Short A D. 1984. Morphodynamic variability of surf zones and beaches: A synthesis. Marine Geology, 56(1–4): 93–118

Xiao Zheyu. 2021. Research on sediment recycling nourishment technology and coastal evolution under influence of artificial island (in Chinese) [dissertation]. Xiamen: Third Institute of Oceanography, Ministry of Natural Resources

Yue Baojing, Liao Jing, Gao Maosheng, et al. 2017. Evolutionary features of morphodynamics of sandy beaches on the Shandong Peninsula. Marine Sciences (in Chinese), 41(4): 118–127

Zhang Linlin. 2014. Study on equilibrium beach nourishment profile and numerical simulation of its evolution (in Chinese) [dissertation]. Tianjin: Tianjin University

Zhou Liangyong, Xue Chunding, Liu Jian, et al. 2013. Beach Morphodynamics and impact factors on the beaches in the Northern and Eastern of Shandong Peninsula. Advances in Marine Science (in Chinese), 31(1): 83–94

Zhu Shibing, Li Zhiqiang. 2019. Study on beach response to Typhoon Khanun (No. 1720) along southern Leizhou Peninsula. Journal of Tropical Oceanography (in Chinese), 38(1): 96–104

Zhu Lei, Yang Yanxiong, Yang Wen, et al. 2019. Study on the response process of nourished beach to “803” storm surge. Marine Science Bulletin (in Chinese), 38(1): 102–114

Zhuang Zhenye, Cao Lihua, Li Bing, et al. 2011. An overview of beach nourishment in China. Marine Geology & Quaternary Geology (in Chinese), 31(3): 133–139